International Journal of the Physical Sciences Vol. 6(33), pp. 7657 - 7668, 9 December, 2011
Available online at http://www.academicjournals.org/IJPS
ISSN 1992 - 1950 ©2011 Academic Journals

Full Length Research Paper

Application of advanced spaceborne thermal emission and reflection radiometer (ASTER) data in geological mapping

Amin Beiranvand Pour and Mazlan Hashim*

Institute of Geospatial Science & Technology (INSTeG), Universiti Teknologi Malaysia, 81310 UTM Skudai, Johor Bahru, Malaysia.

Accepted 7 September, 2011

The spectral and spatial properties of the advanced spaceborne thermal emission and reflection radiometer (ASTER) data can be used in detailed lithological and hydrothermal alteration mapping related to copper and gold mineralization, particularly the shortwave infrared radiation subsystem where hydrothermal alteration minerals have diagnostic spectral absorption features. This paper reviews the technical characteristics of ASTER data and related image processing techniques applicable to ASTER data for lithological and hydrothermal alteration mineral mapping. The hydrothermal alteration zones associated with porphyry copper deposit, such as phyllic, argillic and propylitic, can be discriminated from one another by virtue of their spectral absorption features, which are recognizable by ASTER special bands. The differentiation and identification of phyllic zone are important for exploring porphyry copper mineralization as an indicator of the high potential area with economical mineralization of copper. In this way, we attempt to demonstrate how ASTER remote sensing data can identify and discriminate the hydrothermal alteration zones and lithological units in a regional scale. It is therefore concluded that remote sensing techniques are viable options for geological applications, offering reliable and relatively low cost methods, and could be utilized further to other virgin regions for lithological mapping and for initial steps of mineral exploration.

Key words: Advanced spaceborne thermal emission and reflection radiometer (ASTER), lithological mapping, copper exploration, alteration zones, image processing techniques.

INTRODUCTION

The advanced spaceborne thermal emission and reflection radiometer (ASTER) is a high spatial, spectral and radiometric resolution multispectral remote sensing sensor on national aeronautics and space administration (NASA) earth observing system AM-1 (EOS AM-1) polar orbiting spacecraft. It was launched in December 1999. EOS AM-1 spacecraft operates near polar orbits at 705 km altitude. The recurrent cycle is 16 days. The ASTER instrument is a cooperative effort between the Japanese Ministry of Economic Trade and Industry (METI) and NASA. It has three separate instrument subsystems which provide observations in three different spectral regions of electromagnetic spectrum, including visible and near infrared radiation (VNIR), shortwave infrared radiation (SWIR) and thermal infrared radiation (TIR). The VNIR subsystem has three recording channels between 0.52 and 0.86 µm and an additional backward-looking band for constructing digital elevation models (DEMs) with spatial resolution of 15 m. The SWIR subsystem has six recording channels from 1.6 to 2.43 µm, at a spatial resolution of 30 m, while the TIR subsystem has five recording channels, covering the 8.125 to 11.65 µm wavelength region with spatial resolution of 90 m. ASTER swath width is 60 km (each scene is 60 × 60 km^2) and is useful for regional mapping, but cross-track pointing capability extends the total viewing to 232 km. ASTER sensor can acquire approximately 600 scenes daily (Fujisada, 1995; Abrams and Hook, 1995; Yamaguchi et

*Corresponding author. E-mail: mazlanhashim@utm.my or profmhashim@gmail.com. Tel: +607 -5530666. Fax: +607-5531174.

Table 1. Technical characteristics of ASTER data (Fujisada, 1995; Yamaguchi et al., 1999).

Subsystem	Band number	Spectral range (μm)	Radiometric resolution	Absolute accuracy (σ)	Spatial resolution	Signal quantization
VNIR	1	0.52 - 0.60	NE Δρ ≤ 0.5%	≤ 4%	15 m	8 bits
	2	0.63 - 0.69				
	3N	0.78 - 0.86				
	3B	0.78 - 0.86				
SWIR	4	1.600 - 1.700	NE Δρ ≤ 0.5%	≤ 4%	30 m	8 bits
	5	2.145 - 2.185	NE Δρ ≤ 1.3%			
	6	2.185 - 2.225	NE Δρ ≤ 1.3%			
	7	2.235 - 2.285	NE Δρ ≤ 1.3%			
	8	2.295 - 2.365	NE Δρ ≤ 1.0%			
	9	2.360 - 2.430	NE Δρ ≤ 1.3%			
TIR	10	8.125 - 8.475	NE ΔT ≤ 0.3 k	≤ 3K(200-240K)	90 m	12 bits
	11	8.475 - 8.825		≤ 2K(240-270K)		
	12	8.925 - 9.275		≤ 1K(270-340K)		
	13	10.25 - 10.95		≤ 2K(340-370K)		
	14	10.95 - 11.65				
Stereo base-to-height ratio				0.6 (along-track)		
Swath width				60 km		
Total coverage in cross-track direction by pointing				232 km		
Coverage interval				16 days		
Altitude				705 km		
MTF at Nyquist frequency				0.25 (cross-track) 0.20 (along-track)		
Band to band registration				Intra-telescope: 0.2 pixels Intra-telescope: 0.3 pixels		
Peak power				726 w		
Mass				406 kg		
Peak data rate				89.2 Mbps		

Band number 3N refers to the nadir pointing view, whereas 3B designates the backward pointing view.

al., 1999; Abrams, 2000; Yamaguchi et al., 2001). The technical characteristics of ASTER data are indicated in Table 1. ASTER provides data useful for studying the interaction among the geosphere, hydrosphere, cryosphere, lithosphere and atmosphere of the earth from the geophysical point of view. To be more specific, wide range of science investigations and applications includes: (1) geology and soil; (2) land surface climatology; (3) vegetation and ecosystem dynamics; (4) volcano monitoring; (5) hazard monitoring; (6) carbon cycle and marine ecosystem; (7) hydrology; (8) aerosol and cloud; (9) evapotranspiration rate; and (10) land surface and land cover change (Fujisada, 1995). ASTER standard data products are available 'on-demand' from the Earth Remote Sensing Data Analysis Center (ERSDAC, Japan) and the EROS data center (EDC, USA). Basically, all the

ASTER captured data are processed to generate Level-1A data product. It consists of unprocessed raw image data and coefficients for radiometric correction. The Level-1B (radiance-at-sensor) data product is a re-sampled image data generated from the Level-1A data by applying the radiometric correction coefficients. Level-2B data products of physical parameters including surface radiance data with nominal atmospheric corrections (Level-2B01), surface reflectance data contains atmospherically corrected VNIR-SWIR data (Level-2B07 or AST-07), surface emissivity data with MODTRAN atmospheric correction and a temperature-emissivity separation (TES) algorithm (Level-2B04) are generated on the basis of user request. Level-4B data product is also generated under the user request from the along-track stereo observation in the near infrared channel (band 3N and 3B) in order for the construction of digital elevation models (DEMs). Level-3A is a geometrically well-corrected orthorectified ASTER standard data product with ASTER-driven DEM, which is radiometrically equivalent to Level-1B radiance-at-sensor data (Gillespie et al., 1998; Yamaguchi et al., 1999; Abrams, 2000; Yamaguchi et al., 2001; Ninomiya, 2005, 2003a, b, c). Recently, two new crosstalk-corrected ASTER SWIR reflectance products had been released, which include: (1) AST-07XT SWIR reflectance data product available 'on-demand' from ERSDAC and EDC (Iwasaki and Tonooka, 2005) and (2) RefL1b SWIR reflectance data product complied and introduced (Mars and Rowan, 2010). The AST-07XT SWIR reflectance data product is similar to AST-07 surface reflectance data that consist of VNIR and SWIR bands, except that the crosstalk correction algorithm and atmospheric correction (non-concurrently acquired MODIS water vapor data) have been applied (Iwasaki and Tonooka, 2005; Biggar et al., 2005; Mars and Rowan, 2010). RefL1b and AST-07XT reflectance datasets have crosstalk correction; differences between these datasets should be caused by the addition of the radiometric correction factors and use of concurrently acquired water vapor data in the atmospheric correction of the RefL1b data (Mars and Rowan, 2010). During scene acquisition of ASTER data, there is optical 'crosstalk' effect caused by stray of light from band 4 detector into adjacent band 5 and 9 detectors on SWIR subsystem. Such deviations from correct reflectance result in false absorption features and distortion of diagnostic signatures and consequently misidentification of spectroscopic results. Fortunately, ASTER cross-talk correction software is available in www.gds.aster.ersdac.or.jp (Kanlinowski and Oliver, 2004; Iwasaki and Tonooka, 2005; Hewson et al., 2005; Mars and Rowan, 2006, 2010).

Since 2000, ASTER data have been widely and successfully used in lithological mapping and mineral exploration, because of their characteristics of the spectral properties and the diversity of standard data products (Hewson et al., 2001; Rowan and Mars, 2003; Rowan et al., 2003; Junek, 2004; Hellman and Ramsey, 2004; Galva˜o et al., 2005; Vaughan et al., 2005; Hubbard and Crowly, 2005; Rowan et al., 2005; Mars and Rowan, 2006; Rowan et al., 2006, 2010; Ducart et al., 2006; Qiu et al., 2006; Di Tommaso and Rubinstein, 2007; Khan et al., 2007; Moghtaderi et al., 2007; Kruse and Perry, 2007; Sanjeevi, 2008; Moore et al., 2008; Tangestani et al., 2008; Khan and Mahmood, 2008; Azizi et al., 2010; Amer et al., 2010; Aboelkhair et al., 2010; Gabr et al., 2010; Kratt et al., 2010). ASTER is the first multispectral space-borne instrument that allows discrimination and identification of hydrothermal alteration minerals in the SWIR region of electromagnetic spectrum (Abram and Hook, 1995). Moreover, the ASTER VNIR and TIR data can provide capability for the remote identification of vegetation and iron oxide minerals in surface soil and mapping carbonates and silicates, respectively (Bedell, 2001; Ninomiya, 2003a; Rockwell and Hofstra, 2008). Accordingly, this paper reviews the application of ASTER data for lithological mapping and the identification of hydrothermal alteration mineral zones for the exploration of porphyry copper and epithermal gold deposit.

PORPHYRY COPPER DEPOSIT

Porphyry copper deposits are associated with volcanic-plutonic arcs in subduction environments and paleosubduction zones (Pirajno, 1992). There are several analogous of porphyry copper belts in subduction tectonic setting of the world, such as the Andean Volcanic Belt in Western South America, the Urumieh-Dokhtar Volcanic belt in Iran, Northern Sulawesi in Indonesia, Carpathian-Balkan in Central and South Europe, Yulong-Yunna (Himalaya) in China, Mulong in NSW Australia (Singer et al., 2005). Porphyry copper deposits are usually located within or near plutonic intrusions, formed typically below depths of one kilometer which mostly have rocks of Mesozoic to Cenozoic age (Titley, 1972; Jacobsen, 1975). Porphyry copper deposits, in contrast to other hydrothermal deposits, invariably are associated genetically with porphyry plutons localized along island and continental-arc strike-slip fault system (Titley and Beane, 1981; Carranza and Hale, 2002a). The crustal deformation present near subduction zones may play a significant role in allowing plutons to passively rise to shallow crustal levels (Wolfe, 1988; Tosdal and Jeremy, 2001). Felsic plutonic rocks ranging in composition from quartz monzonite to granodiorite are common ore hosts. However, this type of mineralization can occur in dioritic to syenitic rocks (Rowins, 1999). Porphyry copper deposits are generated by hydrothermal fluid processes that alter the mineralogy and chemistry of the composition of country rocks (Hunt and Ashley, 1979; Ferrier and Wadge, 1996; Ferrier et al., 2002). This alteration can produce distinctive mineral assemblages

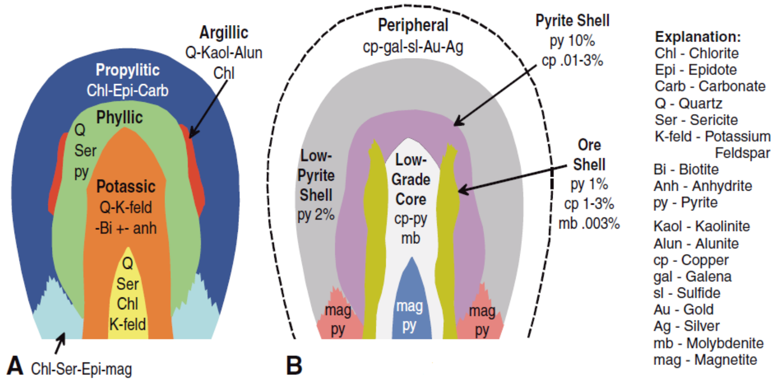

Figure 1. Hydrothermal alteration zones associated with porphyry copper deposit (Modified from Lowell and Guilbert, 1970; Mars and Rowan, 2006). (A) Schematic cross section of hydrothermal alteration mineral zones, which consist of propylitic, phyllic, argillic, and potassic alteration zones. (B) Schematic cross section of ores associated with each alteration zone.

with diagnostic spectral absorption features in the visible near-infrared through the short-wave infrared (0.4 to 2.5 µm) and/or the thermal-infrared (8.0 to 14.0 µm) wavelength regions (Abrams et al., 1983; Abrams and Brown, 1984; Spatz and Wilson, 1995). These absorption features are generated by vibrational processes due to over tones and combination tones of fundamental hydroxyl groups (Hunt and Salisbury, 1974, 1975, 1976; Hunt, 1977). Porphyry copper deposits typically occur in association with hydrothermal alteration mineral zones, such as phyllic, argillic, potassic and propylitic (Lowell and Guilbert, 1970) (Figure 1). A core of quartz and potassium-bearing minerals is surrounded by multiple zones which contain clay and other hydroxyl minerals with diagnostic spectral absorption features in SWIR portion of electromagnetic spectrum. Furthermore, at the same time an oxide zone with extensive iron oxide minerals is developing by virtue of supergene alteration processes over porphyry copper bodies. Iron oxides are one of the important mineral groups that are associated with hydrothermally altered rocks, and are rendered to characteristic yellowish or reddish color to the altered rocks, termed gossan (Sabins, 1999; Abdelsalam and Stern, 2000; Xu et al., 2004). Iron oxide minerals have low reflectance in visible and higher reflectance in near infrared wavelength region (Hunt and Salisbury, 1974; Hunt, 1977). These hydrothermal alteration minerals with diagnostic spectral absorption properties in visible near-infrared through the short-wave infrared can be identified by multispectral remote sensing data as a guide in the initial step of porphyry copper exploration. Remote sensing multispectral sensors with sufficient spectral and spatial resolution such as TM/ETM$^+$ and ASTER are capable of delineating these spectral absorption features, thus can be used to detect and remotely identify these hydrothermal alteration mineral zones in well-exposed regions. Landsat TM/ETM$^+$ data have been used for mineral exploration, because of the two SWIR bands (bands 5 and 7) which were used to detect hydrothermal alteration mineral assemblages associated with epithermal gold and hydrothermal porphyry copper mineralization (Rowan et al., 1977; Podwysocki et al., 1984; Crosta and Moore, 1989; Okada et al., 1993; Sabins, 1996, 1997; Van der Meer et al., 1997; Ruiz-Armenta and Prol-Ledesma, 1998; Abdelsalam and Stern, 2000; Tangestani and Moore, 2002; Carranza and Hale, 2002b; Kusky and Ramadan, 2002; Inzana et al., 2003; Perry, 2004; Yujun et al., 2007). The broad configuration of bands 5 and 7 of TM/ETM$^+$ in the short wave infrared portion just allows the recognition of hydrothermal alteration sites, without providing the essential spectral resolution to discriminate specific alteration zones and minerals, a very important task in searching for high potential prosperous mineralized alteration zone (Gabr et al., 2010).

The six spectral bands of the ASTER SWIR subsystems were designed to measure reflected solar radiation in order to distinguish Al-OH, Fe, Mg-OH, Si-O-H and CO_3 absorption features (Fujisada, 1995; Abram and Hook, 1995). Therefore, the ASTER SWIR reflective bands are capable to identify hydrothermal alteration mineral assemblages that include: (1) mineralogy generated by the passage of low PH fluids (alunite and pyrophylite); (2) Al-Si-(OH) and Mg-Si-(OH)-bearing minerals including kaolinite and mica and chlorite groups; (3) Ca-Al-Si-(OH) bearing minerals including epidote group and also carbonate (calcite and dolomite) as a group (Huntington, 1996). Previous studies have demonstrated the identification of specific hydrothermal alteration minerals, such as alunite, kaolinite, calcite, dolomite, chlorite, talc and muscovite, as well as mineral groups, through analysis of ASTER SWIR data which have

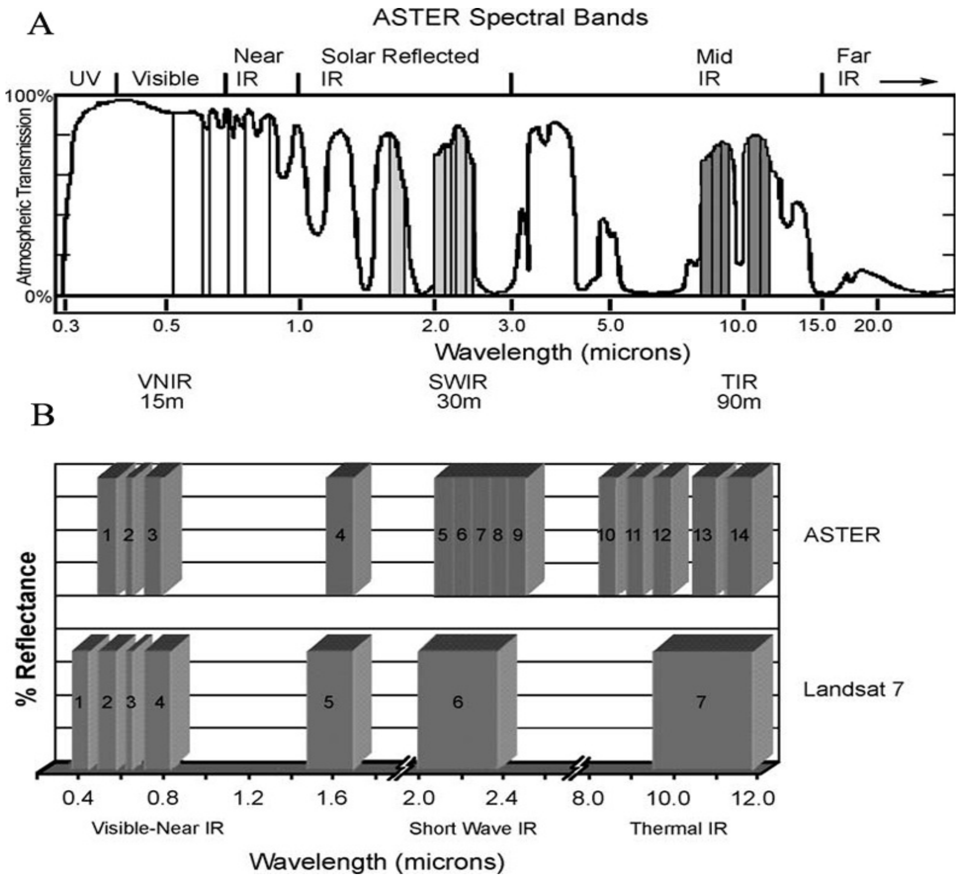

Figure 2. (A) ASTER spectral bands in the wavelength of the electromagnetic spectrum, (B) the comparison of ASTER spectral bands with Landsat-7 TM/ETM$^+$ (Pieri and Abrams, 2004).

have been proven using in situ field spectral measurements (Hewson et al., 2001; Rowan and Mars, 2003; Rowan et al., 2003; Crosta and Filho, 2003; Hubbard et al., 2003; Junek, 2004; Hellman and Ramsey, 2004; Wickert and Budkewistsch, 2004; Galvao et al., 2005; Mars and Rowan, 2006, 2010; Rowan et al., 2006; Ducart et al., 2006; Di Tommaso and Rubinstein, 2007; Sanjeevi, 2008; Azizi et al., 2010; Gabr et al., 2010; Kratt et al., 2010). Figure 2 shows the location of ASTER spectral bands in the wavelength of the electromagnetic spectrum and the comparison of spectral bands between Landsat-7 TM/ETM$^+$ and ASTER. ASTER SWIR spectral properties are unprecedented multispectral data for the discrimination of hydrothermal alteration mineral zones associated with porphyry copper mineralization.

Accordingly, the broad phyllic zone is characterized by illite/muscovite (sericite) that indicate an intense Al-OH absorption feature centered at 2.20 µm coinciding with ASTER band 6, and the narrower argillic zone including, kaolinite and alunite that display a secondary Al-OH absorption feature at 2.17 µm corresponding with ASTER band 5. The mineral assemblage of the outer propylitic zone is epidote, chlorite and calcite that exhibit absorption features situated in the 2.35 µm that coincide with ASTER band 8 (Figure 3) (Hunt, 1977; Hunt and Ashley, 1979; Crowley and Vergo, 1988; Clark et al., 1990; Spatz and Wilson, 1995; Dalton et al., 2004; Mars and Rowan, 2006; Rowan et al., 2006). The differentiation between alteration zones and the identification of phyllic zone are important in the exploration of porphyry copper mineralization, because phyllic zone can be an indicator of high potential prosperous area with economical mineralization of copper ore shell (Figure 1) (Lowell and Guilbert, 1970).

LITHOLOGICAL AND ALTERATION MINERAL MAPPING BY ASTER DATA

The use of ASTER multispectral data in mineral exploration and lithological mapping has increased in recent years due to spectral characteristics of unique integral. ASTER bands is highly sensitive to hydrothermal alteration minerals, especially in SWIR region and the possibility of applying the diversity of image processing techniques, ‘on-demand’ data availability with low cost and broad coverage for regional scale mapping. Here, we review image processing techniques applicable on ASTER

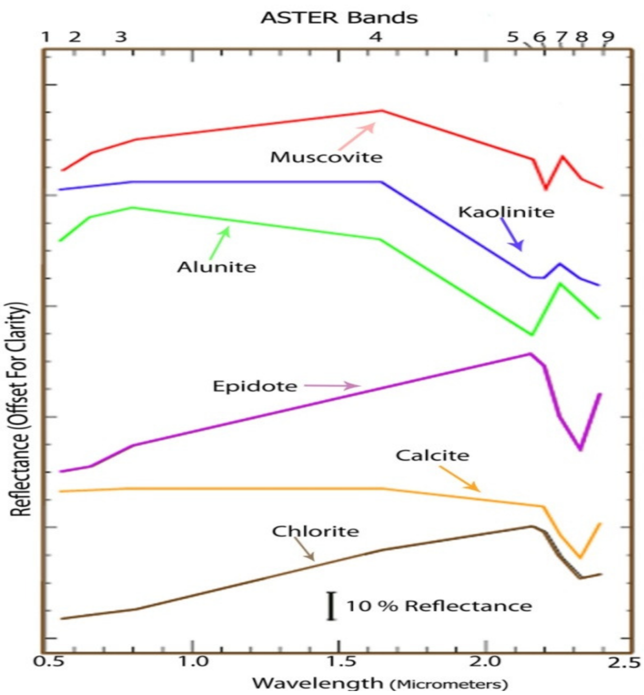

Figure 3. Laboratory spectra of muscovite, kaolinite, alunite, epidote, calcite and chlorite resampled to ASTER band passes. Spectra include muscovite, typical in phyllic alteration zone, with a 2.20 µm absorption feature; kaolinite and alunite, which are common in argillic alteration zone, have 2.17 µm secondary absorption features and epidote, calcite and chlorite, which are typically associated with propylitic alteration zone and display 2.35 µm absorption features (Mars and Rowan, 2006).

data for lithological and hydrothermal alteration mineral mapping as follows.

Hewson et al. (2001) simulated the ability of the ASTER multispectral data for geologic and alteration mineral mapping in Mountain Fitton, South Australia. This test site has been previously surveyed by visible-shortwave hyperspectral automatic modal selection (AMS) (HyMap) and thermal infrared multispectral scanner (TIMS) data sets and several field campaigns collecting relevant spectral measurements. Hewson et al. (2001) applied decorrelation stretch on simulated ASTER bands 3-2-1 so as to the delineation of the drainage and vegetation and band 13-12-10 for the identification of quartz rich areas, respectively. They also implemented mixture tuned matched filtering (MTMF) technique on the simulated ASTER SWIR bands to obtain spectrally unmixed end members related to the rich areas of hydrothermal alteration mineral assemblages. Derived results showed good accuracy in comparison with in situ field spectral measurements and HyMap and thermal infrared multispectral scanner's outputs collected previously.

Rowan et al. (2003) evaluated the capability of the ASTER data for mapping the hydrothermally altered rocks and the country rocks in the Cuprite mining district in Nevada, USA. They used matched filtering (MF) technique for the identification of the surface distribution of hydrothermal alteration minerals. Results indicated that spectral reflectance differences in the nine bands in visible near-infrared through the shortwave infrared (0.52 to 2.43 µm) can provide subtle spectral information for mapping and the discrimination of main hydrothermal alteration mineral zones. They identified silicified zone, opalized zone, argillized zone and the distribution of unaltered country rock units which in comparison with airborne visible/infrared imaging spectrometer (AVIRIS) results demonstrate good agreement. Rowan and Mars (2003) used ASTER data for lithological mapping in Mountain Pass, California, USA. They applied relative absorption-band depth (RBD), matched filtering (MF) and spectral angle mapping (SAM) techniques for the differentiation of calcitic, granodioritic, gneissic, granitic and quartzose rocks. The output results showed similarity between the patterns of the mapped rock units with geologic map of the study area. Yamaguchi and Natio (2003) proposed the spectral indices for lithological discrimination and mapping of surface rock types by using ASTER short wave infrared (SWIR) bands. These consisted of alunite index, kaolinite index, calcite index and montmorillonite index that can be calculated by linear combination of reflectance values of the five SWIR bands.

ASTER has a total of 14 spectral channels; but with spectral ratioing among these selective bands, more lithologic and mineralogic indices and more accurate results can be derived from ASTER image. Ninomiya (2003 a, b) defined vegetation index and mineralogic indices for ASTER VNIR and SWIR bands and lithologic indices for ASTER TIR bands with considering spectral absorption features of vegetation and different minerals and rocks in ASTER spectral channels. These indices are listed as follows:

$$\text{Stabilized Vegetation Index (StVI)} = \left[\frac{band3}{band2}\right]\left[\frac{band1}{band2}\right] \quad (1)$$

$$\text{OH bearing altered minerals Index (OHI)} = \left[\frac{band7}{band6}\right]\left[\frac{band4}{band6}\right] \quad (2)$$

$$\text{Kaolinite Index (KLI)} = \left[\frac{band4}{band5}\right]\left[\frac{band8}{band6}\right] \quad (3)$$

$$\text{Alunite Index (ALI)} = \left[\frac{band7}{band5}\right]\left[\frac{band7}{band8}\right] \quad (4)$$

$$\text{Calcite Index (CLI)} = \left[\frac{band6}{band8}\right]\left[\frac{band9}{band8}\right] \quad (5)$$

$$\text{Quartz Index (QI)} = \frac{(band11 * band11)}{band10 * band12} \quad (6)$$

$$\text{Carbonate Index (CI)} = \frac{band\,13}{band\,14} \quad (7)$$

$$\text{Mafic Index (MI)} = \frac{band\,12}{band\,13} \quad (8)$$

These defined indices are applied on ASTER Level-1B radiance at the sensor data in Cuprite district in Nevada, USA; Yarlung Zangbo ophiolite zone, Tibet; Beishan mountains area, China; North-western Gansu province, China and ophiolite zone in Oman (Ninomiya, 2002, 2003c, 2004). These indices provided accurate information for vegetation, mineral and lithological mapping, and showed the distribution of selected minerals and rocks, satisfactorily. Produced map results indicated excellent spatial coherency and correlate well with the published geology map of the study areas. Crosta et al. (2003) employed principal component analysis (PCA) over ASTER VNIR and SWIR bands for targeting of key alteration minerals associated with epithermal gold deposits in Los Menucos, Patagonia, Argentina. PCA was applied to selected subsets of four ASTER bands according to the position of characteristic spectral absorption features of key hydrothermal alteration mineral end members, such as alunite, illite, smectite and kaolinite in the VNIR and SWIR regions of electromagnetic spectrum. Obtained results revealed that PCA technique can extract detailed mineralogical spectral information from ASTER data for producing abundance images of selected minerals. Thus, this technique can be employed for the identification of hydrothermal alteration minerals in the exploration of precious and base-metal deposits. Volesky et al. (2003) distinguished the propylitic alteration zone and gossan associated with massive sulfide mineralization from the host rock by ASTER (4/2, 4/5 and 5/6) band ratio image in the Neoproterozoic Wadi Bidah shear zone, South-western Saudi Arabia. Xu et al. (2004) identified hydrothermal alteration mineral zones around gold deposits using ASTER data in the North-eastern part of Laizhou region, China. They used PCA technique and band ratio of 3/2, 4/1 and 4/6 for the delimitation of vegetation, iron oxide and clay minerals, respectively.

Hewson et al. (2005) generated maps of Al-OH and Mg-OH/carbonate minerals and ferrous iron content from ASTER SWIR data as well as a map of quartz content from ASTER TIR data for the Broken Hill-Curnamona province of Australia. Rowan et al. (2005) evaluated ASTER band ratio and relative absorption band depth (RBD), matched filtering (MF) and spectral angle mapping (SAM) techniques for lithological mapping of ultramafic complex in the Mordor Pound, NT, Australia. They identified subtle information for the classification of felsic and mafic-ultramafic rocks, alluvial-colluvial deposits and quartzose to intermediate composition rocks. This classification was based on spectral absorption features of Al-OH and ferric-iron mineralogical groups for felsic rock, ferrous-iron and Fe, Mg-OH mineralogical absorption features in mafic-ultramafic rock in the ASTER VNIR+SWIR data and Si-O spectral features for diversity of ultramafic complex and adjacent rocks, such as mafic-ultramafic, quartzose to intermediate composition rocks, alluvial-colluvial deposits and quartzite unite in ASTER TIR data, respectively. Ninomiya et al. (2005) applied quartz index (QI), carbonate index (CI) and mafic index (MI) on ASTER-TIR 'radiance-at-sensor' data for detecting mineralogic or chemical composition of quartzose, carbonate and silicate rocks in Mountain Yushishan, China and Mountain Fitton, Australia. These lithologic indices could discriminate quartz, carbonate and mafic-ultramafic rocks which were compatible with published geologic map and field observation. They also, suggested that these lithologic indices can be one unified approach for lithological mapping of the earth, especially in arid and semi-arid regions.

Galvao et al. (2005) implemented the spectral angle mapping (SAM) technique on the ASTER SWIR bands to investigate the spectral discrimination of hydrothermally altered minerals in a tropical savannah environment in the Northern portion of Gious state, central Brazil. Results showed the efficacy of ASTER SWIR data in discriminating areas of altered minerals from the surrounding vegetation environment. Gomez et al. (2005) estimated the 9 ASTER bands for geological mapping in the Western margin of the Kalahari Desert in Namibia. They realized principal component analysis (PCA) and supervised classification on visible near infrared and short wave infrared ASTER bands. The processing of ASTER data demonstrated validation of the lithological boundaries defined on previous geological map and also provided the information for characterizing new litho-logical units, which were previously unrecognized.

Rowan et al. (2006) identified distribution of hydrothermally altered rocks consisting of phyllically, argillically and propylitically altered zones based on spectral analysis of VNIR+SWIR ASTER bands, as well as hydrothermally silicified rocks were mapped by TIR ASTER bands in the Reko Diq, Pakistan Cu-Au mineralized area. Qui et al. (2006) employed spectral angle mapping (SAM), spectral feature fitting (SFF) and linear spectral unmixing (LSU) techniques on 14 ASTER bands for geological mapping in the Neoproterozoic Allaqi-Heiani suture, Southern Egypt. These techniques have proved to be useful tools in geological mapping. Mars and Rowan (2006) developed logical operator algorithms based on ASTER defined band ratios for regional mapping of phyllic and argillic altered rocks in Zargros magmatic arc, Iran. The logical operator algorithms have illustrated distinctive patterns of argillic and phyllic alteration zones associated with Eocene to Miocene intrusive igneous rocks, as well as known porphyry copper deposits.

Ducart et al. (2006) applied mixture tuned matched filtering (MTMF) technique on ASTER SWIR data to provide regional and local information of the spatial distribution of hydrothermal alteration zones at the Cerro La Mina epithermal gold prospect, Patagonia, Argentina. The main identified alteration zones, such as advanced argillic, argillic and silicic, showed a satisfactory correlation of the spatial distribution with achieved field spectroscopy data. Zhang and Panzer (2007) employed the matched filtering (MF) technique on EO-1 Hyperion and ASTER data to extract abundance images for gold-associated lithological mapping in South-eastern Chocolate Mountain, California, USA. The assessment of matched filtering score index indicated ASTER has good capability in discrimination and classification of rock types. Although, the Hyperion data can produce better accuracy than ASTER, but the lithologic information extracted from ASTER image data is mostly similar with Hyperion results and the better availability and vast spatial coverage make it more suitable for regional scale lithological mapping.

Di Tommaso and Rubinstein (2007) used band ratio and band combination and spectral angle mapping (SAM) techniques for mapping hydrothermal alteration minerals associated with Infiernillo porphyry copper deposit by ASTER data in the San Rafale Massif, Southern Mendoza Province, Argentina. They detected illite, kaolinite, sericite and jarosite through analysis of SWIR bands and surface silica and potassic alteration zone by TIR bands, respectively. Yujun et al. (2007) delineated the hydrothermal alteration anomalies for predicting Cu-Au mineral resources by ASTER data in Oyu Tolgoi, Mongolia. The spectral angle mapping (SAM) and principal component analysis (PCA) techniques are used for alteration anomaly extraction. Gad and Kusky (2007) resolved geological mapping problems by using new ASTER band ratio image 4/7, 4/6 and 4/10 for lithological mapping in the Arabian-Nubian shield, the Neoproterozoic Wadi Kid area, Sinai, Egypt. These ASTER band ratios mapped the main rock units including gneiss and migmatite, amphibolite, volcanogenic sediments with banded iron formation, meta-pelites, talc schist, meta-psammites, meta-acidic volcanics, meta-pyroclastics volcaniclastics, albitites and granitic rocks. Khan et al. (2007) used principal component analysis (PCA), minimum noise fraction (MNF) on VNIR + SWIR ASTER data for lithological mapping in Muslim Bagh ophiolite complex, Pakistan. The PCA discriminated metamorphic sole, sheeted dike complex, basalt and cherts, diabase dikes and gabbro bodies. The MNF transformed data detected sedimentary units, metamorphic sole, laterite, depleted harzburgite and diabase dikes/sills.

Zhang et al. (2007) evaluated ASTER surface reflectance (AST-07) data for gold-related lithological mapping and alteration mineral detection in the South Chocolate Mountains area, California, USA. PCA transformation applied on mineralogic indices include the OH bearing altered minerals index (OHI), kaolinite index (KLI), alunite index (ALI) and calcite index (CLI) for delineating alteration zones. The constrained energy minimization (CEM) technique (a subpixel unmixing algorithm) detected alunite, kaolinite, muscovite and montmorillonite by using ASTER VNIR and SWIR surface reflectance data and reference spectra from the ASTER spectral library. Moghtaderi et al. (2007) used ASTER data for distinguishing sodic-calcic, potassic and silicic-phyllic alteration patterns associated with hydrothermal iron oxide deposits in the Chadormalu paleocrater, Bafq region, Central Iran. The alteration minerals identified by implementing false color composite (FCC), decorrelation-stretch, minimum noise fraction transform (MNF), correlated filter and mathematical evaluation method (MEM) techniques on ASTER data.

Massironi et al. (2008) processed the ASTER data for geological mapping and granitoids detection in the Saghro massif, Eastern Anti-Atlas, Morocco. False color composites (FCC), band ratios, and principal component analysis (PCA) employed on VNIR/SWIR and TIR data for detecting major lithological contacts and mineralized faults. The supervised maximum-likelihood classifications (MLL) and spectral angle mapping (SAM) were carried out on VNIR/SWIR data for discriminating granitoid rocks. Rockwell and Hofstra (2008) used ASTER thermal infrared emissivity data for the identification of quartz and carbonate minerals in Northern Nevada, USA. Quartz index (QI) and carbonate index (CI) were implemented on ASTER Level 2 surface emissivity (Level-2B04) data for geologic mapping and mineral resource investigations. Mapping hydrothermal quartz and carbonate rocks at regional and local scales have considerable economical attention for ore deposit exploration, because these rocks can be host rock for wide range of metallic ore deposit types.

Tangestani et al. (2008) evaluated ASTER Level-1B ‘radiance-at-sensor’ and surface reflectance (AST-07) data for alteration zone enhancement associated with porphyry copper mineralization in Northern Shahr-e-Babak, Iran. Directed principal component analysis (DPCA) and spectral angle mapping (SAM) techniques detected illite, chlorite and muscovite minerals. Sanjeevi (2008) investigated the potential of linear spectral unmixing (LSU) technique over ASTER VNIR/SWIR data for targeting and quantification of mineral content in limestone and bauxite rich areas in Southern India. The results, not only target limestone and bauxite accurately, but also estimate the quality of these deposits. Moore et al. (2008) mapped mineralogical alteration associated with gold deposits by using ASTER Level 1A data in the Takab area, North-west Iran. They applied selective principal component analysis, relative absorption band-depth and matched filtering methods for argillic and silicic alteration mapping.

Amer et al. (2010) suggested new ASTER band ratios (2+4)/3, (5+7)/6 and (7+9)/8 for mapping ophiolitic rocks (serpentinites, metagabbros and metabasalts) in the

Central Eastern Desert of Egypt. Principal component analysis (PCA) was also applied for discrimination between ophiolitic rocks and grey granite and pink granite. The achieved results from field works verified the accuracy and potential of these techniques for lithological mapping in arid and semi-arid regions. Kratt et al. (2010) analyzed ASTER VNIR and SWIR band combinations using decorrelation stretch algorithm for identifying areas of hydrothermally altered rock and tufa deposition in Pyramid Lake, Nevada, USA. Aboelkhair et al. (2010) used ASTER Level 1B 'radiance-at-sensor'and Level 2B04 'surface emissivity' TIR bands for mapping albite granite in the Central Eastern Desert of Egypt. Running band ratio and band combination and quartz index (QI) allowed the discrimination of albite granite from other rock types in the study area.

Gabr et al. (2010) detected areas of high potential gold mineralization using ASTER surface reflectance (AST-07) data in Abu-Marawat, North-eastern Desert of Egypt. Spectral discrimination between high-potential and low-potential areas of gold mineralization recognized by implementing of PCA transformed mineral indices, a band ratio derived from the image spectra (4/8, 4/2 and 8/9 in RGB), constrained energy minimization (CEM) and spectral angle mapping (SAM) techniques. The results of field investigations proved the accuracy of these image processing techniques. Mars and Rowan (2010) assessed two new ASTER SWIR surface reflectance data products, namely RefL1b and AST-07XT for spectroscopic mapping of rocks and minerals. Results indicated that these new ASTER products are more capable than previous ASTER products in discriminating hydrothermal alteration minerals and mineral groups without using additional spectral data from the site for calibration.

Pour et al. (2011) discriminated hydrothermal alteration zones associated with porphyry copper mineralization using ASTER data in Urumieh-Dokhtar volcanic belt, South-eastern Iran. They applied spectral mapping techniques; including spectral angle mapper (SAM), linear spectral unmixing (LSU), matched filtering (MF) and mixture tuned matched filtering (MTMF) on shortwave infrared radiation (SWIR) bands of ASTER. Spectral mapping techniques discriminated the phyllic, argillic and propylitic alteration zones, as well as highlighting the phyllic zone as indicator of high-potential area of Cu mineralization. Pour and Hashim (2011) investigated the spectral transformation of ASTER bands using principal component analysis (PCA), minimum noise fraction (MNF) and band ratioing methods in two major copper mining districts of South-eastern Iran. PC images and associated statistics factors yielded by PCA transformation were detected vegetation and iron oxide minerals using the visible and near infrared radiation (VNIR) bands, clay minerals in the shortwave infrared radiation (SWIR) bands and silicate rocks in the thermal infrared radiation (TIR) bands of the ASTER data, respectively. The PCA results were verified by comparison with obtained results by minimum noise fraction and band ratio methods and also prior knowledge about the study area.

CONCLUSIONS

This paper reviews the application of ASTER remote sensing data in mineral exploration aspects for mapping and for identification of lithology and hydrothermal alteration minerals related to porphyry copper and epithermal gold mineralization. Unprecedented spectral characteristics of ASTER multispectral data provide and improve the remote sensing information for reconnaissance stages of mineral exploration. The applicability of diversity of image processing techniques on ASTER data allows the extraction of substantial information which is useful for geological applications. The availability and diversity of ASTER standard data products make them the best remote sensing data for exploration geologists. It is well-known that the porphyry copper deposit is characterized by: (1) the presence in subduction tectonic setting; (2) permanent association with volcanic-plutonic arcs and (3) occurrence in association with hydrothermal alteration mineral zones. These significant characteristics can be marker for exploration of porphyry copper deposits; especially, recognizing hydrothermally altered rocks by their diagnostic spectral absorption signatures in shortwave infrared region of electromagnetic spectrum through ASTER remote sensing data is considered to be of prime importance. Hydrothermal alteration zones associated with porphyry copper deposit, such as phyllic, argillic, potassic and propylitic can be discriminated from one another by their spectral absorption features which are recognizable by ASTER special bands. The differentiation between phyllic, argillic and propylitic zones, which can be presented in many geologic environments associated with porphyry copper mineralization, can be critical in the initial steps of copper exploration. With respect to surface hydrothermal alteration mineral mapping for porphyry copper exploration, the identification of phyllic zone as an indicator of high potential prosperous mineralized lithologic unit is important. Techniques and achievements reviewed in this paper can further introduce the usefulness of ASTER data for future exploration of porphyry copper deposits. Currently, porphyry copper deposits with low grade copper and broad in scope provide nearly three-quarters of world's Cu in world metal market. They are also significant host for gold and molybdenum which are extracted as precious by-product.

ACKNOWLEDGEMENTS

This study was conducted as part of Fundamental Research Grant Scheme, Ministry of Higher Education

Malaysia. We are grateful to the Universiti Teknologi Malaysia for providing the facilities and finance for this investigation. The authors would like to thank reviewers for their helpful and constructive reviews of this manuscript.

REFERENCES

Abdelsalam M, Stern R (2000). Mapping gossans in arid regions with landsat TM and SIR-C images, the Beddaho Alteration Zone in northern Eritrea. J. Afr. Earth Sci., 30(4): 903-916.

Aboelkhair H, Yoshiki N, Yasushi W, Isao S (2010). Processing and interpretation of ASTER TIR data for mapping of rare-metal-enriched albite granitoids in the Central Eastern Desert of Egypt. J. Afr. Earth Sci., 58(1): 141-151.

Abrams M, Brown D, Lepley L, Sadowski R (1983). Remote sensing of porphyry copper deposits in Southern Arizona. Ecol. Geol., 78: 591–604.

Abrams M, Brown D (1984). Silver Bell, Arizona, porphyry copper test site report: Tulsa, Oklahoma, The American Association of Petroleum Geologists, The Joint NASA–Geosat Test Case Project, Final Report, chapter 4, p. 4-1-4-73.

Abrams M, Hook SJ (1995). Simulated ASTER data for geologic studies. IEEE Tran. Geol. Rem. Sens., 33(3).

Abrams M (2000). The Advanced Spaceborne Thermal Emission and Reflection Radiometer (ASTER): data products for the high spatial resolution imager on NASA's Terra platform. Int. J. Rem. Sens., 21: 847-859.

Amer R, Kusky T, Ghulam A (2010). Lithological mapping in the Central Eastern Desert of Egypt using ASTER data. J. Afr. Earth Sci., 56: 75-82.

Azizi H, Tarverdi MA, Akbarpour A (2010). Extraction of hydrothermal alterations form ASTER SWIR data from east Zanjan, Northern Iran. Adv. Spa. Res., 46: 99-109.

Bedell RL (2001). Geological mapping with ASTER satellite: new global satellite data that is a significant leap in remote sensing geologic and alteration mapping. Spec. Publication Geol. Society of Nev., 33: 329–334.

Biggar SF, Thome KJ, McCorkel JT, D'Amico JM (2005). Vicarious calibration of the ASTER SWIR sensor including crosstalk correction. Proceedings Int. Society Opt. Eng., 5882-588217.

Carranza EJ, Hale M (2002a). Where are porphyry copper deposits spatially localized? A case study in Benguet province, Philippines. Natural Res. Res., 11(1): 45-59.

Carranza EJ, Hale M (2002b). Mineral mapping with Landsat Thematic Mapper data for hydrothermal alteration mapping in heavily vegetated terrane. Int. J. Rem. Sens., 23(22): 4827-4852.

Clark RN, King TVV, Klejwa M, Swayze GA (1990). High spectral resolution reflectance spectroscopy of minerals. J. Geophy. Res., 95: 12653-12680.

Crosta A. Moore JM (1989). Enhancement of Landsat Thematic Mapper imagery for residual soil mapping in SW Minais Gerais State, Brazil: a prospecting case history in Greenstone belt terrain. In: Proceedings of the 7th ERIM Thematic Conference: Remote sens. explor. geol., pp. 1173-1187.

Crosta AP, Filho SCR, Azevedo F, Brodie C (2003). Targeting key alteration minerals in epithermal deposits in Patagonia, Argentina, Using ASTER imagery and principal component analysis. Int. J. Rem. Sens., 24: 4233-4240.

Crosta AP, Filho SCR (2003). Searching for gold with ASTER. Earth. Observ. Mag., 12 (5): 38–41.

Crowley JK, Vergo N (1988). Near-infrared reflectance spectra of mixtures of kaolin group minerals: use in clay mineral studies. Clays. Clay. Miner., 36: 310-316.

Dalton JB, Bove DJ, Mladinich CS, Rockwell BW (2004). Identification of spectrally similar materials using the USGS Tetracorder algorithm: the calcite-epidot-chlorite problem. Rem. Sen. Environ., 89: 455- 466.

Di Tommaso I, Rubinstein N (2007). Hydrothermal alteration mapping using ASTER data in the Infiernillo porphyry deposit, Argentina. Ore. Geol. Rev., 32: 275-290.

Ducart DF, Crosta AP, Filho CRS (2006). Alteration mineralogy at the Cerro La Mina epithermal prospect, Patagonia, Argentina: field mapping, short-wave infrared spectroscopy, and ASTER images. Ecol. Geol., 101: 981-996.

Ferrier G, Wadge G (1996). Application of imaging spectrometry data to mapping alteration zones associated with gold mineralization in southern Spain. Int. J. Rem. Sens., 17: 331-350.

Ferrier G, White K, Griffiths G, Bryant R, Stefouli M (2002). The mapping of hydrothermal alteration zones on the island of Lesvos, Greece, using an integrated remote sensing data set. Int. J. Rem. Sens., 23: 341–356.

Fujisada H (1995). Design and performance of ASTER instrument. In: Breckinridge, J.B. (Ed.), Proceedings Int. Soc. Opt. Eng., 2583: 16-25.

Gabr S, Ghulam A, Kusky T (2010). Detecting areas of high-potential gold mineralization using ASTER data. Ore. Geo. Rev., 38: 59-69.

Gad S, Kusky T (2007). ASTER spectral ratioing for lithological mapping in the Arabian–Nubian shield, the Neoproterozoic Wadi Kid area, Sinai, Egypt. Gond. Res., 11: 326-335.

Galva˜o LS, Almeida-Filho R, Vitorello I.C (2005). Spectral discrimination of hydrothermally altered materials using ASTER short-wave infrared bands: Evaluation in a tropical savannah environment. Int. J. Appl. Ear. Observ. Geoinformation, 7: 107-114.

Gillespie AR, Matsunaga T, Rokugawa S, Hook SJ (1998). Temperature and emissivity separation from Advanced Spaceborne Thermal Emission and Reflection Radiometer (ASTER) images. IEEE Trans. Geosci. Rem. Sens., 36: 1113–1126.

Gomez C, Delacourt C, Allemand P, Ledru P, Wackerle R (2005). Using ASTER remote sensing data set for geological mapping, in Namibia. Phys. Chem. Earth., 30: 97-108.

Hellman MJ, Ramsey MS (2004). Analysis of hot springs and associated deposits in Yellowstone National Park using ASTER and AVIRIS remote sensing. J. Volcan.Geothe. Res., 135: 195- 219.

Hewson RD, Cudahy TJ, Huntington JF (2001).Geological and alteration mapping at Mt Fitton, South Australia, using ASTER satellite-borne data. IEEE Trans. Geosci. Rem. Sens., pp. 724-726.

Hewson RD, Cudahy TJ, Mizuhiko S, Ueda K, Mauger AJ (2005). Seamless geological map generation using ASTER in the Broken Hill–Curnamona province of Australia. Rem. Sen. Environ. 99: 159-172.

Hubbard BE, Crowley JK, Zimbelman, DR (2003). Comparative alteration mineral mapping using visible to shortwave infrared (0.4-2.4 µm) Hyperion, ALI, and ASTER imagery. IEEE Trans. Geosci. Rem. Sens., 41(6): 1401-1410.

Hubbard BE, Crowley JK (2005). Mineral mapping on the Chilean–Bolivian Altiplano using co-orbital ALI,ASTER and Hyperion imagery: Data dimensionality issues and solutions. Rem. Sen. Environ., 99: 173-186.

Hunt GR, Salisbury JW (1974). Mid-infrared spectral behavior of igneous rocks. Technical Report AFRCL-TR-75-0356, US Air Force Cambridge Research Laboratory, Cambridge, MA.

Hunt GR, Salisbury JW (1975). Mid-infrared spectral behavior of sedimentary rocks. Technical Report AFRCL-TR-75-0356, US Air Force Cambridge Research Laboratory, Cambridge, MA.

Hunt GR, Salisbury JW (1976). Mid-infrared spectral behavior of metamorphic rocks, Technical Report AFRCL-TR-76-0003, US Air Force Cambridge Research Laboratory, Cambridge, MA.

Hunt GR (1977). Spectral signatures of particulate minerals in the visible and near infrared. Geophy., 42: 501-513.

Hunt GR, Ashley P (1979). Spectra of altered rocks in the visible and near infraraed. Ecol. Geol., 74: 1613-1629.

Huntington JF (1996). The role of remote sensing in finding hydrothermal mineral deposits on Earth. Evolution of Hydrothermal Ecosystems on Earth (and Mars?). Wiley, England, pp. 214-234.

Inzana J, Kusky T, Higgs G, Tucker R (2003). Supervised classifications of Landsat TM band ratio images and Landsat TM band ratio image with radar for geological interpretations of central Madagascar. J. Afr. Earth Sci., 37: 59-72.

Iwasaki A., Tonooka H (2005). Validation of a crosstalk correction algorithm for ASTER/SWIR. IEEE Trans. Geosci. Rem. Sens., 43(12): 2747-2751.

Jacobsen JBJ (1975). Copper deposits in time and space. Min. Sci.

Eng., 7 (4): 337–371.
Junek P (2004). Geological mapping in the Cheleken Peninsula, Turkministan area using Advanced Spaceborne Thermal Emission and Reflection Radiometer (ASTER) data, ISPRS conference.
Kanlinowski A, Oliver S (2004). ASTER Mineral Index Processing. Remote Sensing Application Geoscience Australia. Aust. Government Geoscience Website: http://www.ga.gov.au/image_cache/GA7833.pdf.
Khan SD, Mahmood K, Casey JF (2007). Mapping of Muslim Bagh ophiolite complex (Pakistan) using new remote sensing, and field data. J. Asian Earth Sci., 30: 333-343.
Khan SD., Mahmood K (2008). The application of remote sensing techniques to the study of ophiolites. Earth.Sci. Rev., 89: 135-143.
Kratt C, Calvin WM, Coolbaugh MF (2010). Mineral mapping in the Pyramid Lake basin: Hydrothermal alteration, chemical precipitates and geothermal energy potential. Rem. Sens. Environ. 114(10): 2297-2304.
Kruse FA, Perry SL (2007). Regional mineral mapping by extending hyperspectral signatures using multispectral data. IEEE Trans. Geos. Rem. Sens., 4: 1-14.
Kusky T, Ramadan TM (2002). Structural controls on Neoproterozoic mineralization in the South Eastern Desert, Egypt: an integrated field, Landsat TM, and SIR-C/X SAR approach. J. Afr. Earth Sci., 35: 107-121.
Lowell JD, Guilbert JM (1970). Lateral and vertical alteration-mineralization zoning in porphyry ore deposits: Economic Geol. and the Bulletin of the Soc. Ecol. Geol., 65(4): 373-408.
Mars JC, Rowan LC (2006). Regional mapping of phyllic- and argillic-altered rocks in the Zagros magmatic arc, Iran, using Advanced Spaceborne Thermal Emission and Reflection Radiometer (ASTER) data and logical operator algorithms. Geosphere, 2(3): 161-186.
Mars JC, Rowan LC (2010). Spectral assessment of new ASTER SWIR surface reflectance data products for spectroscopic mapping of rocks and minerals. Rem.Sens.Environ., 114: 2011-2025.
Massironi ML, Bertoldi P, Calafa D, Visona A, Bistacchi C, Giardino A, Schiavo B (2008). Interpretation and processing of ASTER data for geological mapping and granitoids detection in the Saghro massif (eastern Anti-Atlas, Morocco). Geosphere., 4(4): 736 -759.
Moghtaderi A, Moore F, Mohammadzadeh A (2007). The application of advanced space-borne thermal emission and reflection (ASTER) radiometer data in the detection of alteration in the Chadormalu paleocrater, Bafq region, Central Iran. J. Asian. Earth Sci., 30: 238–252.
Moore F, Rastmanesh F, Asady H, Modabberi S (2008). Mapping mineralogical alteration using principal component analysis and matched filter processing in Takab area, north-west Iran, from ASTER data. Int. J. Rem. Sens., 29(10): 2851-2867.
Ninomiya Y, Fu B (2002). Mapping quartz, carbonate minerals and mafic–ultramafic rocks using remotely sensed multispectral thermal infrared ASTER data. Proceedings of SPIE, 4710: 191-202.
Ninomiya Y (2003a). A stabilized vegetation index and several mineralogic indices defined for ASTER VNIR and SWIR data. Proc. IEEE 2003 International Geoscience and Remote Sensing Symposium (IGARSS'03) v. 3, Toulouse, France, 21–25 July 2003, pp.1552-1554.
Ninomiya Y (2003b). Advanced remote lithologic mapping in ophiolite zone with ASTER multispectral thermal infrared data. Proc. IEEE 2003 International Geoscience and Remote Sensing Symposium (IGARSS'03) v. 3, Toulouse, France, 21–25 July 2003, pp.1561-1563.
Ninomiya Y (2003c). Rock type mapping with indices defined for multispectral thermal infrared ASTER data: case studies. Proceedings of SPIE, 4886: 123-132.
Ninomiya Y (2004). Lithological mapping with ASTER TIR and SWIR data. Proceedings of SPIE., 5234: 180-190.
Ninomiya Y, Fu B, Cudahy TJ (2005). Detecting lithology with Advanced Spaceborne Thermal Emission and Reflection Radiometer (ASTER) multispectral thermal infrared “radiance-at-sensor” data. Rem. Sen. Environ., 99 (1-2): 127-139.
Okada K, Segawa K, Hayashi I (1993). Removal of the vegetation effect from LANDSAT TM and GER imaging spectroradiometer data. ISPRS J. Photo. Rem. Sens., 48 (6): 16-27.
Pirajno F (1992). Hydrothermal mineral deposits: Principal and fundamental concepts for the exploration geologist. Springer-Verlag, Berlin, p. 709.
Perry SL (2004). Spaceborne and airborne remote sensing systems for mineral exploration-case histories using infrared spectroscopy. In: King, P.L., Ramsey, M.S., Swayze, G.A. (Eds.), Infrared Spectroscopy in Geochemistry, Exploration Geochemistry, and Remote Sensing. MAC, Lond., Can., pp. 227-240.
Pieri D, Abrams M (2004). ASTER watches the world’s volcanoes: a new paradigm for volcanological observations from orbit. J. Volca. Geoth. Res., 135: 13-28.
Podwysocki MH, Mimms DL, Salisbury JW, Bender LV, Jones OD (1984). Analysis of Landsat-4 TM data for lithologic and image mapping purpose, Proceedings of Landsat-4 Science Investigations Summary, Greenbelt, Maryland, 2: 35-39.
Pour B A, Hashim M, Marghany M (2011). Using spectral mapping techniques on short wave infrared bands of ASTER remote sensing data for alteration mineral mapping in SE Iran. Int. J. Phys. Sci., 6(4): 917-929.
Pour BA, Hashim M (2011). Spectral transformation of ASTER and the discrimination of hydrothermal alteration minerals in a semi-arid region, SE Iran. Int. J. Phys. Sci., 6(8): 2037-2059.
Qiu F, Abdelsalam M, Thakkar P (2006). Spectral analysis of ASTER data covering part of the Neoproterozoic Allaqi-Heiani suture, Southern Egypt .J. Afr. Earth Sci., 44: 169–180.
Rockwell B W, Hofstra AH (2008). Identification of quartz and carbonate minerals across northern Nevada using ASTER thermal infrared emissivity data Implications for geologic mapping and mineral resource investigations in well-studied and frontier areas. Geosphere., 4(1): 218–246.
Rowan LC, Goetz AFH, Ashley RP (1977). Discrimination of hydrothermally altered and unaltered rocks in visible and near infrared multispectral images. Geophy., 42 (3): 522–535.
Rowan LC, Mars JC (2003). Lithologic mapping in the Mountain Pass, California area using Advanced Spaceborne Thermal Emission and Reflection Radiometer (ASTER) data. Rem. Sen. Environ., 84: 350-366.
Rowan LC, Hook SJ, Abrams M, Mars JC (2003). Mapping hydrothermally altered rocks at Cuprite, Nevada, using the Advanced Spaceborne Thermal Emission and Reflection Radiometer (ASTER), a new satellite-imaging system. Ecol. Geol., 98(5): 1019-1027.
Rowan LC, Mars JC, Simpson CJ (2005). Lithologic mapping of the Mordor N.T, Australia ultramafic complex by using the Advanced Spaceborne Thermal Emission and Reflection Radiometer (ASTER). Rem. Sen. Environ., 99: 105-126.
Rowan LC, Robert GS, John C (2006). Distribution of hydrothermally altered rocks in the Reko Diq, Pakistan mineralized area based on spectral analysis of ASTER data. Rem. Sens. Environ., 104: 74-87.
Rowins SM (1999). Reduced porphyry copper-gold deposits: a newly recognized style of gold mineralization: GSA Abstract with program, 31(7): A92.
Ruiz-Armenta JR, Prol-Ledesma RM (1998). Techniques for enhancing the spectral response of hydrothermal alteration minerals in Thematic Mapper images of Central Mexico. Int. J. Rem. Sens., 19: 1981-2000.
Sabins FF(1996). Remote Sensing Principles and Interpretation, third ed. Freeman & Co, New York, USA.
Sabins FF (1997). Remote sensing strategies for mineral exploration. In: Rencz, A.E. (Ed.), Remote Sensing for the Earth Sciences. John Wiley & Sons, Inc., New York, pp. 375-447.
Sabins FF (1999). Remote sensing for mineral exploration. Ore. Geol. Rev., 14: 157-183.
Sanjeevi S (2008). Targeting limestone and bauxite deposits in Southern India by spectral unmixing of hyperspectral image data. The International Archives of the Photogrammetry, Remote Sensing and Spatial Information Sciences. Vol 37. Part B8. Beijing 2008.
Singer DA, Berger VI, Menzie WD, Berger BR (2005). Porphyry Copper Deposit Density. Ecol. Geol., 100: 491–514.
Spatz DM, Wilson RT (1995) Remote sensing characteristics of porphyry copper systems, western America Cordillera, *in* Pierce, F.W., and Bolm, J.G., eds.: Arizona Geological Society Digest, 20: 94-108.
Tangestani MH, Moore F (2002). "Porphyry copper alteration mapping

at the Meiduk area, Iran", Int. J. Rem. Sens., 23 (22): 4815-4825.

Tangestani MH, Mazhari N, Ager B, Moore F (2008) Evaluating advance spaceborne thermal emission and reflection radiometer (ASTER) data for alteration zone enhancement in a semi-arid area, northern Shahr-e-Babak, SE Iran. Int. J. Rem. Sens., 29(10): 2833-2850.

Titley SR (1972). Intrusion and Wallrock porphyry copper deposits: Economic Geology and the Bulletin of the Society of Ecology Geology, 67: 122.

Titley SR, Beane RE (1981). Porphyry copper deposits- Part I: Geological settings, petrology and tectogenesis. Eco. geol. 75th Anniversary, Special Volume: 214-235.

Tosdal RM, Jeremy R (2001). Magmatic and structural controls on the development of porphyry Cu or Mo or Au deposits. Eco. Geol., 14: 157-181.

Van der Meer F, Vasquez-Torres M, Van Dijk, PM (1997). Spectral Characterization of Ophiolite Lithologies in the Troodos Ophiolite Complex of Cyprus and its Potential in rospecting for Massive Sulphide Deposits. Int. J. Rem. Sens., 18(6): 1245-1257.

Vaughan RG, Hook SJ, Calvin WM, Taranik JV (2005). Surface mineral mapping at Steamboat Springs, Nevada, USA, with multi-wavelength thermal infrared images. Rem. Sen. Environ., 99: 140-158.

Volesky JC, Stern RJ, Johnson PR (2003). Geological control of massive sulfide mineralization in the Neoproterozoic Wadi Bidah shear zone, southwestern Saudi Arabia, inferences from orbital remote sensing and field studies. Preca. Res., 123 (2-4): 235-247.

Wickert LM, Budkewtisch P (2004). ASTER a geological mapping tool for Canada's north. Case study: the Becher Island, Hudson Bay, Nunavut,Canada. IEEE Trans. Geosci. Remote Sens., pp. 1300-1303.

Wolfe JA (1988). Arc magmatism and mineralization in North Luzon and its relationship to subduction at the East Luzon and North Manila Trenches. South. Asian Earth Sci., 2(2): 79-93.

Xu Y, Qizhong L, Yun S, Lu W (2004). Extraction Mechanism of Alteration Zones using ASTER Imagery. IEEE Trans. Geosci. Remote Sens., pp. 4174-4175.

Yamaguchi YI, Fujisada H, Kudoh M, Kawakami T, Tsu H, Kahle AB, Pniel M (1999). ASTER instrument characterization and operation scnorio. Adv. Spa. Res., 23(8): 1415-1424.

Yamaguchi YI, Fujisada H, Kahle AB, Tsu H, Kato M, Watanabe H, Sato I, Kudoh M (2001). ASTER instrument performance, operation status, and application to Earth sciences. IEEE Trans. Geosci. Rem. Sens., pp. 1215-1216.

Yamaguchi Y, Naito C (2003). Spectral indices for lithologic discrimination and mapping by using the ASTER SWIR bands. Inter. J. Rem. Sens., 24(22): 4311-4323.

Yujun Z, Jianmin Y, Fojun Y (2007). The potentials of Multi-spectral Remote Sensing Techniques for Mineral Prognostication – Taking Mongolian Oyu Tolgoi Cu-Au Deposit as an Example. Earth Sci. Frontiers, 14(5): 63-70.

Zhang X, Pazner M, Norman D (2007). Lithologic and mineral information extraction for gold exploration using ASTER data in the south Chocolate Mountains (California). J. Photo. Rem. Sens., 62: 271-282.

Zhang X, Pazner M (2007). Comparison of lithologic mapping with ASTER, Hyperion, and ETM data in the Southeastern Chocolate Mountains, USA. Phot. Eng. Rem. Sens., 73(5): 555-561.